Nonlinear Optical Methods to Study Condensed Phase Chemical and Biological Dynamics

G. Fleming
University of California, Berkeley, California Institute for Quantitative Biosciences (QB3) & Lawrence Berkeley National Laboratory

1. What's Different About Condensed Phase Dynamics?

Systems in the condensed phase are subject to a variety of different environments that influence the frequencies (energies) of the optical transitions. Furthermore, these environments fluctuate rapidly, reorganize around new electronic or nuclear configurations, and induce changes of electronic state, chemical constitution etc. (Figure 1). The dynamical information is often hidden behind a mask of spectral broadening resulting from these influences, and this makes linear spectroscopy (i.e. absorption spectra) of limited value for the study of condensed phase chemical and biological dynamics.

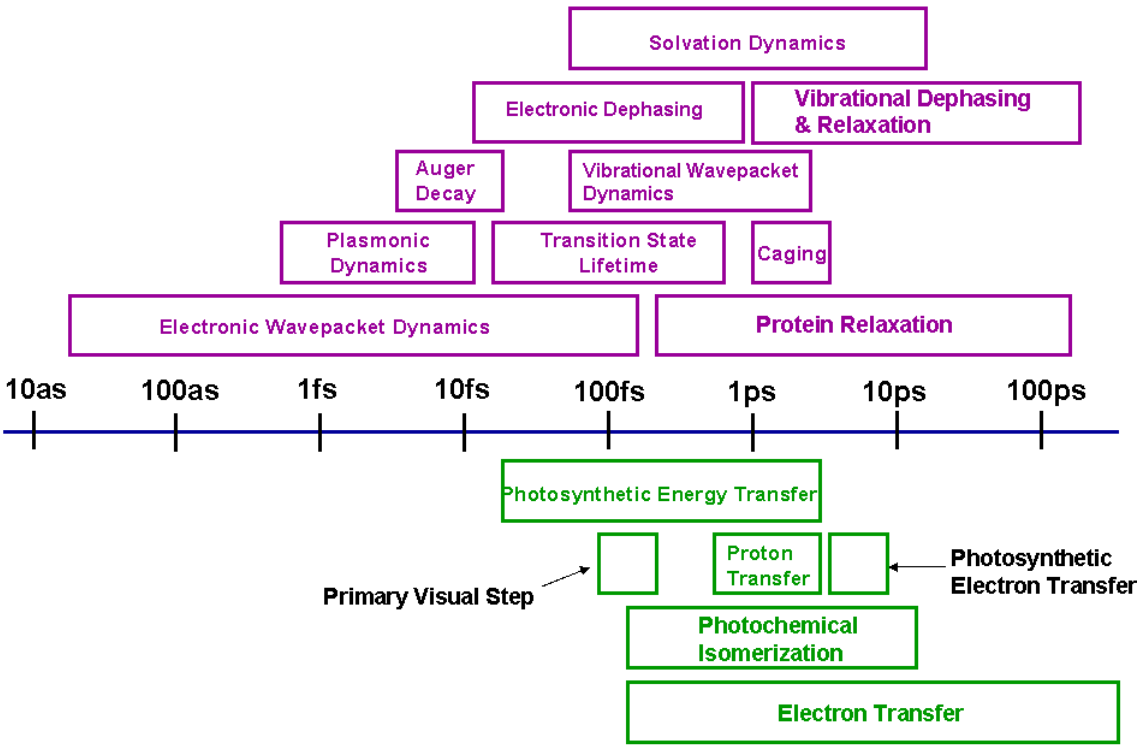

Figure 1 Timescales of Physical and Chemical Phenomena in Condensed Phases

Vibrational frequencies are generally less influenced by differing environments than electronic transition frequencies and when short excitation pulses are used well-defined vibrational wavepackets are created. By short I mean the spectral bandwidth of the pulse is broad enough to span two or more states of the vibrational quantum modes in question. The classical Franck principle asserts that the optical excitation takes place at those wavelengths that conserve the nuclear kinetic energy. This means that a mapping exists between the wavelength of the transition and the nuclear coordinate which, for a diatomic, is simply the bond length (Figure 2).

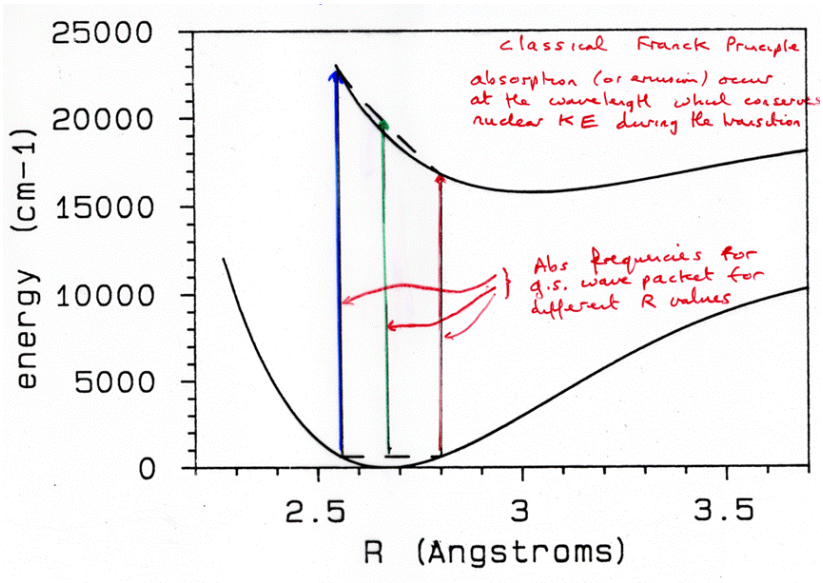

Figure 2 Difference potentials for B←X Absorption of Iodine. Note that different wavelengths correspond to different I-I bond lengths.

A striking example of this comes from iodine, I_2, in hexane solution where the electronic spectrum is entirely featureless, yet clear vibrational wavepackets are observed from both ground and excited states (Figure 3). The excited state wavepacket damps out very rapidly due to dissociation on the excited surface. This dissociation is induced by the solvent, and occurs with very low yield in the gas phase. By changing the probe wavelength, the dissociating wavepackets can be followed out to distances of ~ 4.25 Å, showing that in a room temperature liquid, the dissociative motion is ballistic out to this distance. Around this point, collisions with solvent molecules occur and so iodine atoms recoil and recombine with their original partners. This is called the cage effect (Figure 3b).

The reorganization of a solvent around a newly formed state, such as an electronically excited state created by a short optical pulse, can be followed by means of a time-dependent shift in the fluorescence spectrum--the time-dependent Stokes shift. The response can be characterized by a Stokes shift function S(t), which at ambient temperature, under the conditions of linear response, is equivalent to a correlation function, M(t), constructed as follows: Consider the transition frequency of a particular molecule, *i* (Figure 4a). It consists of an average value related to its chemical nature, $< \omega_{eg} >$, an offset from the average relating to its specific environment, ε_i, and a component that fluctuates as a result of motions of the environment (and the nuclear motions of the system itself), $\delta\omega_{eg}(t)$.

$$\omega^i_{eg}(t) \quad = < \omega_{eg} > + \delta\omega^i_{eg}(t) + \varepsilon_i .$$

The distribution of ε_i values, $f(\varepsilon_i)$, gives the inhomogeneous distribution. If the fluctuations of molecule i are typical of the system we can write

$$M(t) \quad = \frac{< \delta\omega_{eg}(t) \ \ \delta\omega_{eg}(0) >}{< \delta\omega_{eg}{}^2 >}$$

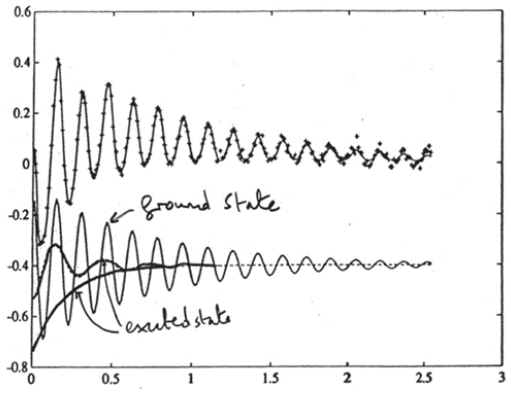

$$S(t) = \sum A_i \cos(\omega_i t - \phi_i)\exp(-t_d/\tau_i)$$

A	ω(cm^{-1})	φ°	τ(fs)	
-0.16	111	-5	210	Excited State
-0.43	0	0	180	Excited State
0.21	211	4	940	Ground State
0.32	0	0	1350	Ground State
0.04	424	-19	900	Ground State

Figure 3a (Top): Transient dichroism signal for I_2 in hexane 580 nm pump, 580 nm probe and decomposition into signals from ground (long-lived oscillations) and excited state (short lived oscillations and exponential decay). Bottom: Singular value description of signal. The exponential component for the ground state arises from rotation of the I_2. The second harmonic of the ground state frequency is also seen at 424 cm $^{-1}$.

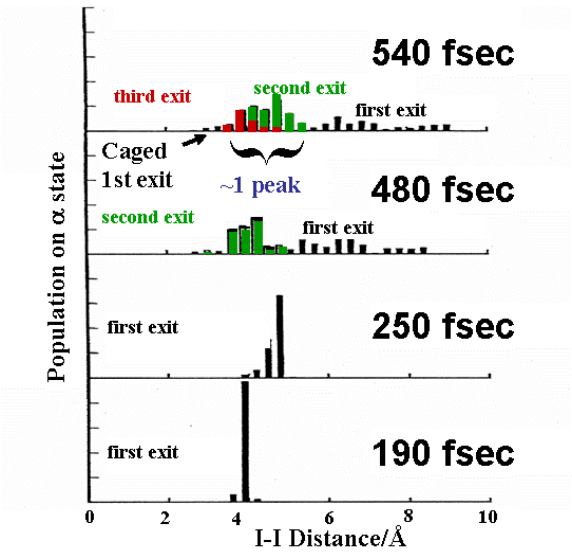

Figure 3b Simulations of I_2 dissociation dynamics in argon solvent. Plotted are histograms of population on the dissociative a state as a function of I-I distance. Note how population from the first exit has reversed direction and has moved to shorter I-I distances at 540 fs. [9].

In an ensemble of chromophores, the dynamics for an individual chromophore (i) can be expressed as $\omega_{eg}^{i}(t) = \langle \omega_{eg} \rangle + \delta\omega_{eg}(t) + \varepsilon_i$

Full width half maximum of $f(\varepsilon)$ = inhomogeneous width

Optical lineshapes and echo measurements relate to:

$$M(t) = \frac{\langle \delta\omega(0)\delta\omega(t) \rangle}{\langle \delta\omega^2 \rangle}$$

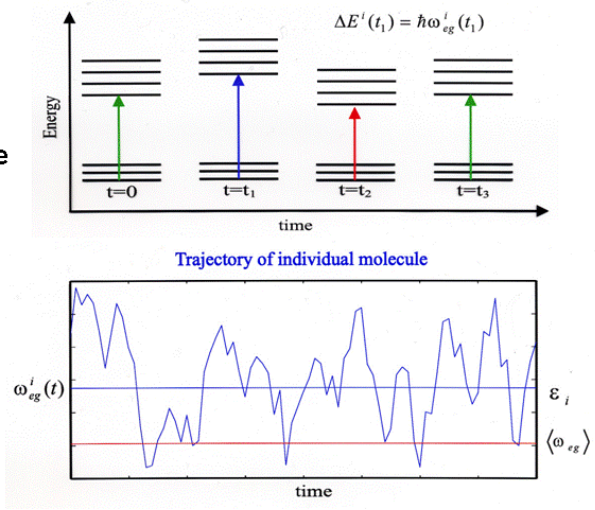

Figure 4a Condensed phase spectral dynamics

Figure 5 shows the time-dependent Stokes shift S(t) (Figure 4b) observed for a dye molecule coumarin 343 in water. Water has the fastest relaxation of any solvent, but other highly polar liquids such as acetonitrile or methanol also have large-amplitude, very rapid (100-200 fs) initial relaxations followed by slower components.

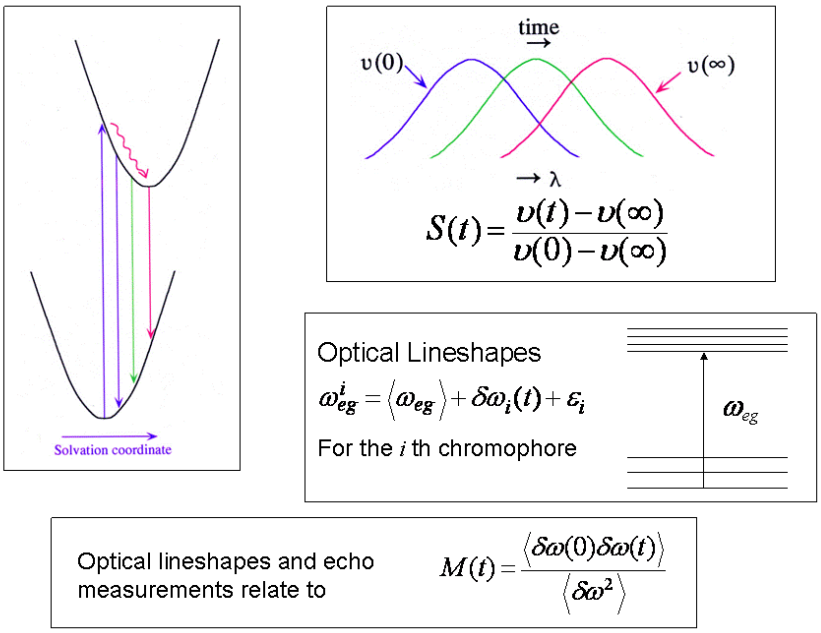

Figure 4b The Stokes shift and solvation dynamics

In order to remove (or even utilize) the influence of inhomogeneous broadening of optical spectra, it is necessary to apply a more sophisticated technique than straightforward pump-

probe spectroscopy or time-resolved fluorescence spectroscopy. To see how this works we need to go a little more deeply into nonlinear spectroscopy.

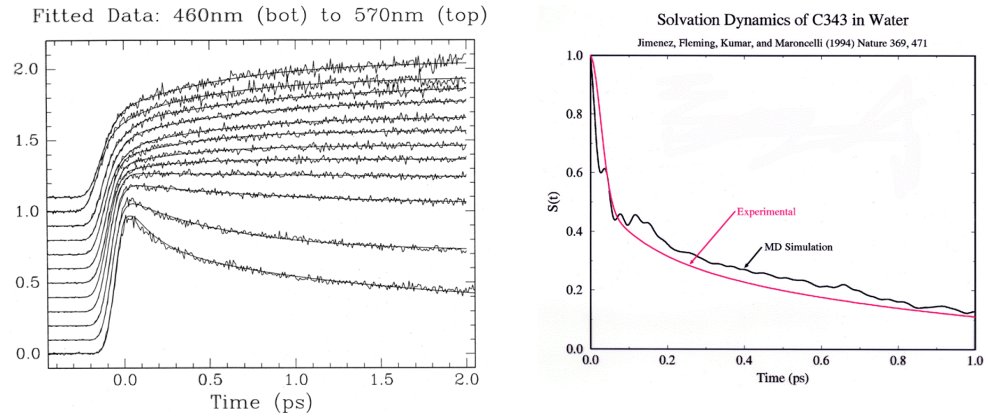

Figure 5 Time resolved fluorescence spectra for Coumarin 343 in water (left) and Stokes shift function calculated from these dyes along with simulated Stokes shift (right) [10].

2. Nonlinear Spectroscopy

Optical spectroscopic experiments are classified according to their power-law dependence on the light field. The quantity responsible for generating a signal is the polarization, *P*, written as

$$P = P^{(1)} + P^{(2)} + P^{(3)} + P^{(4)} + P^{(5)} + \ldots$$

even powers of *P* vanish in centrosymmetric media. $P^{(1)}$ describes the linear response (i.e. absorption, reflection, refraction, propagation). The third order nonlinear response ($P^{(3)}$) will be the one we focus on in this lecture. Equivalently, many experiments can be thought of as n-wave mixing. The third-order non-linear response is four-wave mixing and the signal (ω_s , wavevector k_s) is subject to the following conservation statements

$$\omega_s = \pm\omega_1 \pm \omega_2 \pm \omega_3$$

and when the transition wavelength λ << than the sample size

$$k_s = \pm k_1 \pm k_2 \pm k_3$$

By using three laser pulses to probe a system and detecting at a specific signal direction k_s, one can follow the dynamics of the quantum system as a function of time delays between the pulses.] The quantum dynamics of a condensed phase system is most conveniently described not by the Schrödinger equation, but by the quantum Liouville equation which describes the evolution of the density matrix, $\rho(t)$:

$$i\hbar \frac{\partial}{\partial t} \rho(t) = [H,\rho(t)] \qquad (1)$$

where [,] denotes a commutator and ρ is defined as follows:

The system is an ensemble of systems each with a probability to be in various quantum states $|\Psi_k(t)\rangle$ then ρ

$$\rho = \sum_k P_k |\Psi_k(t)\rangle\langle\Psi_k(t)| \qquad (2)$$

with P_k the probability of finding the system in the state $|\Psi_k(t)\rangle$. If we expand $|\Psi(t)\rangle$ in a basis set $\{|n\rangle\}$ so that $|\Psi(t)\rangle = \sum_n c_n(t)|n\rangle$ and $\langle\Psi(t)| = \sum_m c_m^*(t)\langle m|$ then ρ has matrix elements

$$\rho_{nm} = \sum_k P_k \langle n|\Psi_k\rangle\langle\Psi_k|m\rangle$$

where the diagonal elements (ρ_{nn} etc.) describe populations and the off-diagonal elements (ρ_{nm} etc.) are known as coherences

Describing a non-linear optical experiment is conceptually straightforward (though technically rather complex). The essential idea is that the system starts in a thermal equilibrium density matrix (where the probabilities are given by the Boltzmann factors), has a series of interactions with the light field (three for third order signals), and propagates under its Hamiltonian (which includes both system and system-bath interaction Hamiltonians) during the periods between the interactions. The polarization is then calculated by acting from the left with the dipole operator and taking the trace [2].
The form of the density matrix in equ (2) suggests a diagram that is helpful in visualizing and organizing non-linear experiments--the double-sided Feynman diagram in which the propagation of the ket and bra are depicted separately.

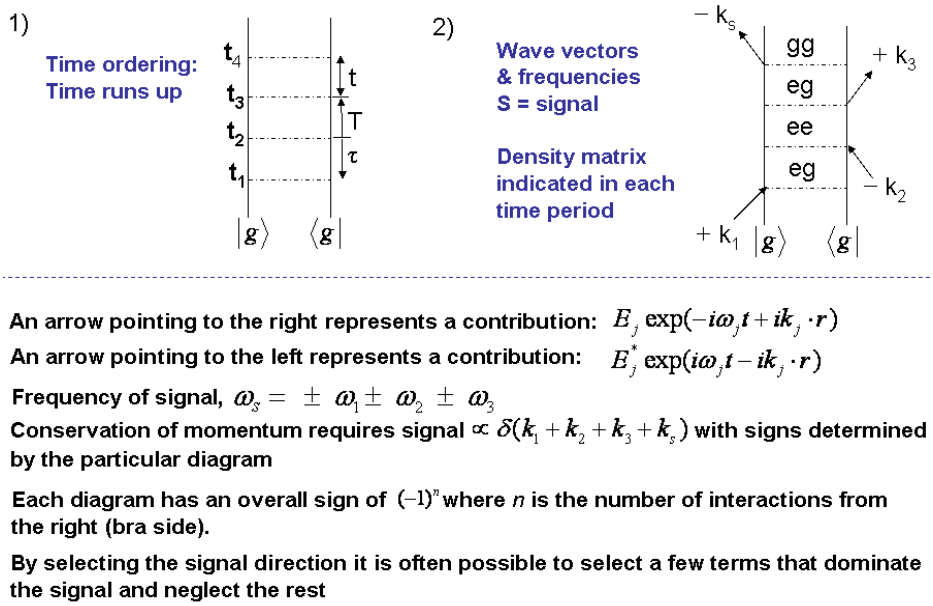

Figure 6 Double-sided Feynman diagrams and rules for their construction.

Figure 6 gives a set of rules for constructing the diagrams and some simple examples. The diagram also gives the direction of the signal field represented by the diagram. For example, linear absorption or linear dispersion give a signal wavevector $k_s = k_1$, while a pump-probe experiment gives a $k_s = k_2$, the probe pulse direction. The central portion of the diagram contains information on the density matrix during that time interval. For a two-level system (levels *g* and *e* for ground and excited) the density matrix is

$$\rho = \begin{pmatrix} \rho_{gg} & \rho_{ge} \\ \rho_{eg} & \rho_{ee} \end{pmatrix}$$

with the diagonal elements describing populations and the off-diagonal elements describing coherences. From equ(1) we find that for a system without coupling to the bath and relaxation between levels (with Hamiltonian H_0)

$$i\hbar\frac{d}{dt}\rho_{gg}(t) = 0 = i\hbar\frac{d}{dt}\rho_{ee}(t)$$

$$i\hbar\frac{d}{dt}\rho_{ge}(t) \quad = \quad (E_g - E_e)\rho_{ge}$$

$$\text{or } \rho_{ge}(t) \quad = \quad \exp((i/\hbar)(E_e - E_g)) \ \times \ \rho_{ge}(0)$$

The coherences oscillate at the Bohr frequency of the system. When relaxation is added to this picture (so that the Hamiltonian, $H = H_0 + H_R$) we find that both populations and coherences decay in a mutually dependent fashion. If we assume simple exponential decay of population and an additional, pure dephasing term for the coherences we can (ignoring notational niceties) write a propagator for the ge coherence as

$$G_{ge}(t_1) \quad = \quad \exp(-i\omega_{ge}t_1 - \Gamma_{ge}t_1) \qquad (3)$$

where the first term in the exponent comes from H_0 and the second from H_R.

$$\text{Here } \Gamma_{ge} \quad = \quad 1/2(\gamma_e + \gamma_g) + \hat{\Gamma}_{ge}$$

with γ_i^{-1} the lifetime of e or g ,and $\hat{\Gamma}_{ge}$ the pure dephasing rate. Γ_{ge} is often written as $1/T_2$, with $\gamma_e = 1/\mathrm{T}_{1,}$ and $\hat{\Gamma}_{ge} = 1/\mathrm{T}_2^*$.

Now consider the diagram labeled R_2 in Figure 7 which describes the following sequence of events (reading from right to left)

$$G_{eg}(t_3)G_{ee}(t_2)G_{ge}(t_1)\rho_g$$

The trace (sum of diagonal elements) of such a matrix quantity is called a response function, in this case conventionally called R_2

$$R_2(t_3, t_2, t_1) \quad = \quad Tr[G_{eg}(t_3)G_{ee}(t_2)G_{ge}(t_1)\rho_g]$$

Note that there are two coherence and one population period, and that the second coherence is the complex conjugate of the first.

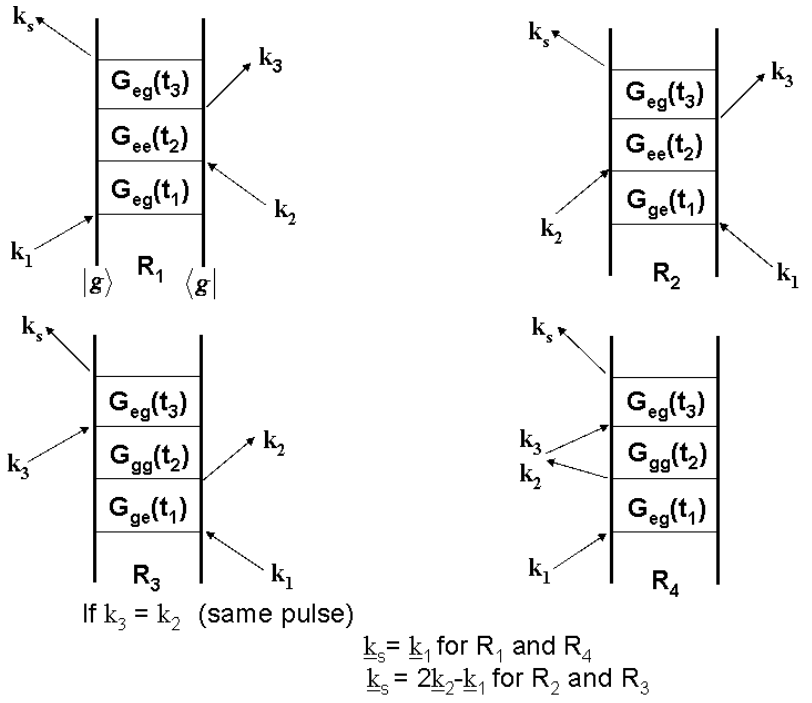

Figure 7 Two level systems are described by four Feynman diagrams and their complex conjugates.

To simplify things let's assume that we do the experiment with two pulses, both of which are very short, and the second of which interacts twice with the system if we choose to detect the signal in the direction $k_s = 2k_2 - k_1$, and the time interval between these two interactions goes to zero. The evolution of the system will be governed by the consecutive action of the two propagators $G_{ge}(t_1)$ and $G_{eg}(t_3)$ (In this case t_2 is set to zero).

Here $G_{ge}(t_1)$ can be written as in equ (3) which is equivalent to

$G_{ge}(t_1) = \exp(+i\omega_{eg}t_1 - \Gamma_{eg}t_1)$

since $\omega_{eg} = -\omega_{ge.}$

If we return to the expression for the transition frequency and (for the moment) ignore the fluctuating term, we have

$\omega_{eg} = <\omega_{eg}> + \varepsilon_{eg} = -\omega_{ge}$

Then the combined action of the two propagators

$$G_{cg}(t_3)G_{ge}(t_1) = \exp(-i<\omega_{eg}>(t_3 - t_1)) \times \exp(-\Gamma_{eg}(t_3 + t_1)) \times \exp(-i\varepsilon_{eg}(t_3 - t_1)) \qquad (4)$$

This is just for one molecule. Now consider a distribution of frequencies in the ensemble, and assume $f(\varepsilon_{eg})$ is a Gaussian with width Δ. Then the last term in equ (4) for the ensemble becomes

$$\int_{-\infty}^{\infty} d\varepsilon_{eg} \exp\left(\frac{-\varepsilon_{eg}^2}{\Delta}\right) \exp\ (-i\varepsilon_{eg}(t_3 - t_1))$$

If Δ is very large, the Gaussian term becomes unity and we are left with

$$\int_{-\infty}^{\infty} d\varepsilon_{eg} \exp(-i\varepsilon_{eg}(t_3 - t_1))$$

This is the integral representation of the Dirac delta function $\delta(t_1 - t_3)$. Thus the elapsed time when $t_3 = t_1$ is the only time where the third term is (4) is nonzero. In other words at $t_3 = t_1$, we get a signal and the inhomogeneous contribution $(f(\varepsilon_{eg}))$ is removed. This signal is the photon echo. We could go on and calculate the decay of the echo signal as we increase t_1. For the very simple model we have used here, the echo decays as $\exp(-4\Gamma_{eg}t)$ if the inhomogeneous broadening is very large. If we look at the first diagram (R_1) in Figure 7 we note two things: (1) the second coherence period is the same as the first and $G_{eg}(t_3)G_{eg}(t_1)$ does not lead to an echo (we call this a non-rephasing sequence), and (2) $k_s = k_1$, so in the limit of very short pulses this signal is spatially distinct from the echo signal at $k_s = 2k_2 - k_1$. Returning to the echo signal we might guess that for less extreme cases of inhomogeneous broadening the echo will be smeared out in time and because of this we will see, very shortly, interesting consequences. It should also be clear that the fluctuations described by $\delta\omega_{eg}(t)$ or $M(t)$ for the ensemble will also influence the echo signal significantly.

3. Real Systems—the Peak Shift Method

Now we add back a finite middle time period to carry out a three-pulse photon echo experiment as shown in Figure 8. By convention we label t_1 as τ, t_2 as T (the population or waiting time), and t_3 as t. In the simplest case the intensity of the echo signal is detected as τ is scanned for fixed values of T. In this case the signal is

$$I(\tau, T) \propto \int_0^\infty dt \left| R(\tau, T, t) \right|^2 \qquad (5)$$

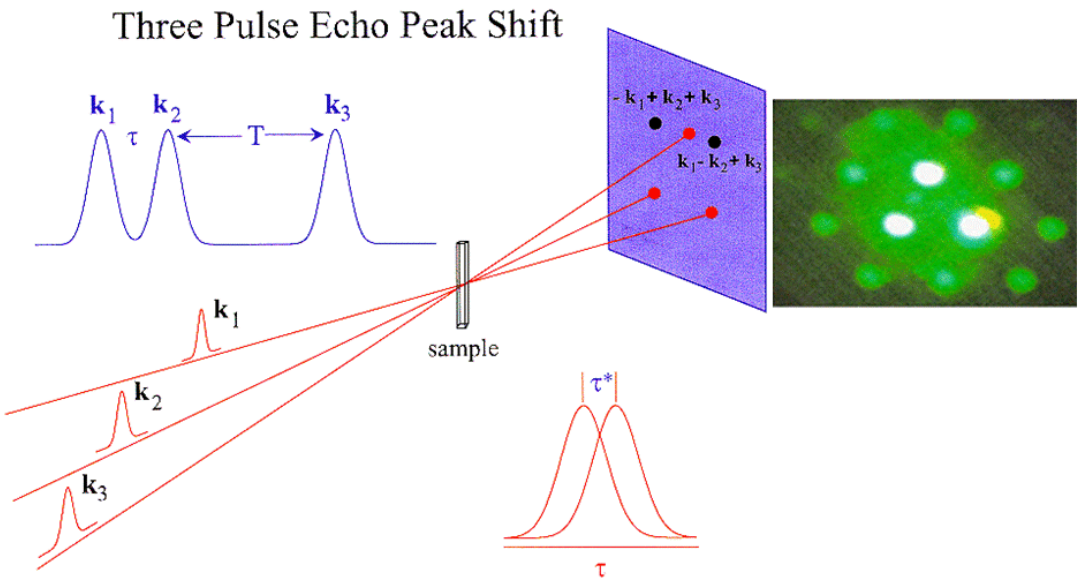

Figure 8 The three-pulse echo. The photograph shows actual data indicating the various phase matched signals generated. The two three-pulse echo signals are indicated by black spots on the screen in the experimental layout.

Representative signals for three different values of T for the dye Nile blue dissolved is acetonitrile are shown in Figure 9 as a function of τ. (Note that in Figure 8 there are two symmetrically related signals $k_s = k_2 + k_3 - k_1$ and $k_s = -k_2 + k_3 + k_1$ around $\tau = 0$ (positive τ means pulse 1 arrives first, negative τ means pulse two comes first). Both signals are plotted in Figure 9. The echo signals themselves in Figure 9 are very nearly symmetric (fits to a Gaussian function are shown) meaning that it would be very difficult to extract dynamical information from fits to the echo decay. However the signals, for small values of T, do not peak at $\tau = 0$. The reasons for this effect are described at length in ref [11], but simply put because the conditions behind our simple derivation do not hold, the echo signal has a finite width and, for small values of $\tau(t_1)$, a portion of the echo is forbidden by causality because the echo width places it *before* pulse 3! Since, as equ (5) shows, we are measuring the area under the echo signal, because of the causality effect the area increases as τ increases even though the maximum amplitude of the echo decreases. For $\tau < 0$, we have a non-rephasing sequence (Figure 10) and the signal always peaks at $\tau = 0$. For long enough times when fluctuations have destroyed the memory of the transition frequency, rephasing (echo generation) is no longer possible and, as Figure 9 shows, the signal becomes symmetric around $\tau = 0$.

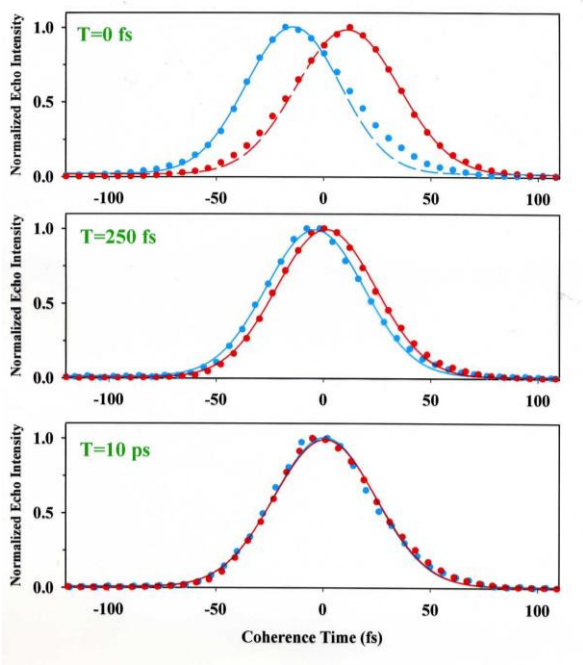

Figure 9 Integrated three pulse photon echoes for Nile Blue at three populations times in acetonitrile.

We can characterize these dynamics by a quantity we call the peak shift or $\tau^*(\mathrm{T})$, the shift of the integrated echo signal maximum from $\tau = 0$. This is most accurately measured by taking half the separation of the two echo signals in Figure 9 since they must be symmetric around $\tau = 0$ at all times.

Figure 11 shows the peak shift vs. population time for the same dye molecule IR144 in dilute solution in ethanol at 294K, in a polymer glass (PMMA) at 294K, and at 32K. The oscillating features in the plot come from vibrational wavepackets as described in Section 1, and will not be discussed further. Note the similarity of the ethanol and PMMA 294K data up to ~160 fs. Simply put it takes ethanol 160 fs to realize it is a liquid and can change its structure to accommodate the excited dye molecule. Eventually (on a 50 ps timescale) the peak shift decays to zero in ethanol as a result of diffusive motions at times larger than ~200 fs. In other words, the system becomes homogeneous when the probe (IR144) has sampled all possible environments. In PMMA, however, static inhomogeneous broadening remains for as long as we care to look. The peak shift goes to a finite value (~ 5.75 fs) and remains there. This long time value then reflects the width of the inhomogeneous distribution. At lower temperature the whole curve shifts to higher $\tau^*(\mathrm{T})$ values. This is largely because the amplitude of the fluctuations, $<\delta\omega^2>^{1/2}$, is reduced at lower temperature, and rather roughly the initial peak shift is inversely proportional to the amplitude of the fluctuations.

The whole peak shift curve can be described using models for $M(t)$ obtained either from computer simulation, sophisticated dielectric response theories, or more empirical approaches such as the Brownian oscillator model. Rather then pursue these approaches we will apply the peak shift method to rather more complex systems—photosynthetic light harvesting complexes.

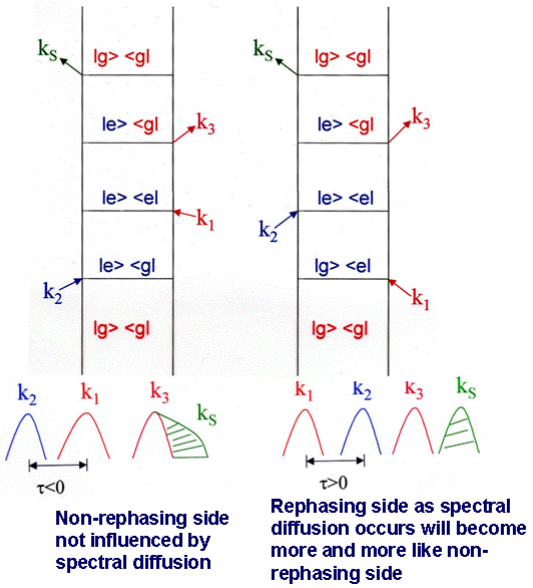

Figure 10 Feynman diagrams illustrating he origin of the peak shift and the reason it decays with increasing population time.

The purple bacterial photosynthetic unit shown in Figure 12 in idealized form on the right and in an AFM image on the left, consists of multiple LH2 rings (with 27 BChl) in contact either with each other or with the LH1 ring that surrounds and eventually transfers the absorbed excitation energy to the reaction center. The various timescales marked in Figure 12 were determined by pump-probe and photon echo spectroscopy. Note that the slowest step is the final one—transfer from LH1 to the reaction center.

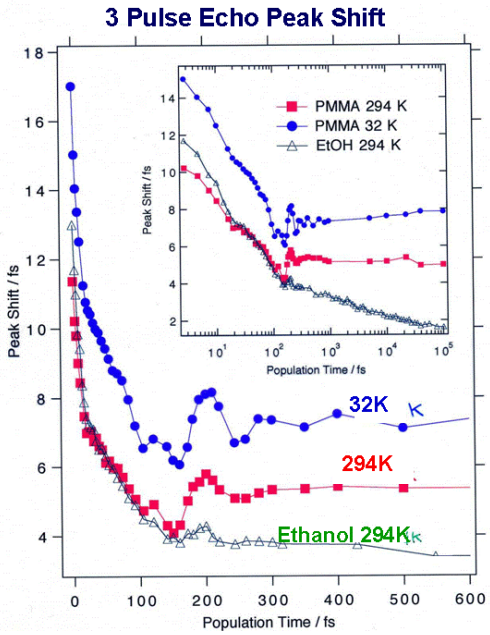

Figure 11 Three-pulse echo peak shift data for the dye IR 144 in two environments in a fluid solvent (ethanol) and a polymer glass at two temperatures. The inset shows data out to longer population times (note the logarithmic timescale).

Figure 13 shows the structure of the LH1 light harvesting complex surrounding the reaction center of a purple bacterium. LH1 contains 32 bacteriochlorophyll (BChl) molecules which present a challenge to the measurement of energy flow within the ring since all the molecules are chemically identical. However, there are fluctuations (inhomogeneous broadening) of the site energies of the individual BChl molecules and this suggests that the photon echo peak shift (3PEPS) could be used to determine the dynamics. 3PEPS data for LH1 are shown in Figure 14 (solid circles). The very rapid (90 fs) decay seen in these data is ascribed to energy transfer observed by the loss of memory of the initial transition frequency as the excitation moves from site to site. This picture is confirmed by the data on the B820 subunit of LH1 also shown in Figure 14 (solid squares). The B820 subunit consists of just one pair of BChl molecules and two α – helices obtained by applying detergent to LH1. The solid lines through the two data sets in Figure 14 are calculated with identical parameters, except that for B820 the rate of energy transfer is set to zero.

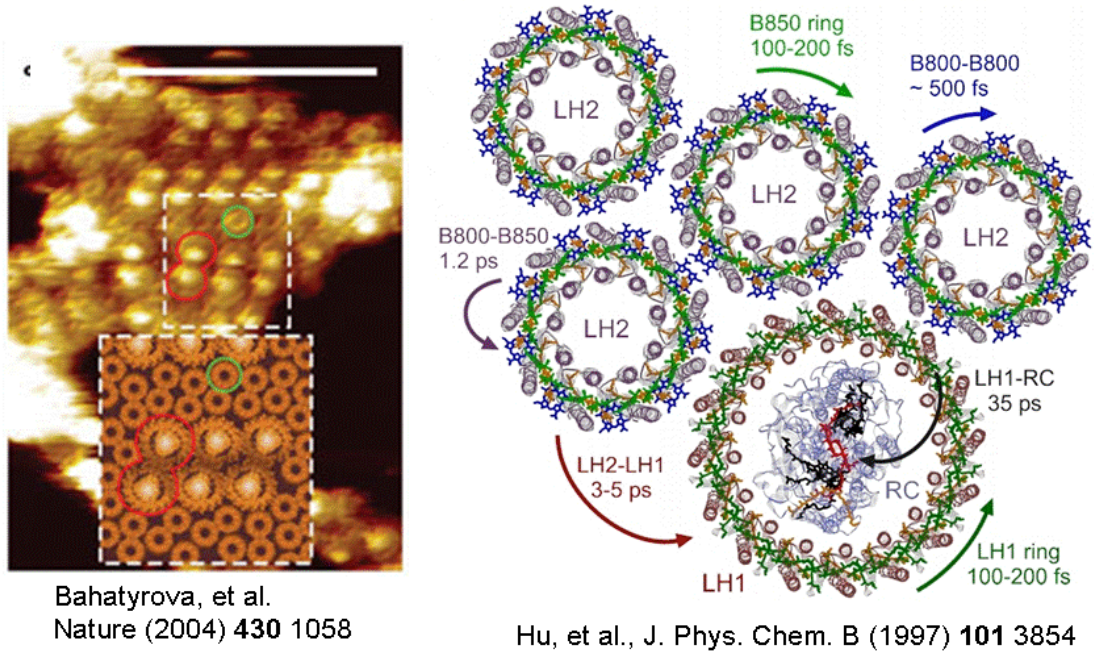

Figure 12 The photosynthetic inset of a purple bacterium.

It should be noted that the peak shift of the LH1 sample in Figure 14 does not decay to zero, but to a fixed value of ~3 fs. This implies that the energy transfer around a single LH1 does not average over the entire disorder of the ensemble—each individual LH1 ring contains a large fraction, but not all, of the possible site energies. This raises the possibility in a photosynthetic unit (Figure 12) with multiple light harvesting complexes that it may be possible to measure the transfer of excitation energy both within and between light harvesting complexes.

LH2 contains two rings of BChl molecules—one of 18 BChl absorbs at 850 nm, and a second of 9 BChl absorbs at 800 nm, approximately the transition wavelength of monomeric BChl in solution. The shift to 850 nm comes about through electronic interactions between the BChls and spectral shifting from two hydrogen bonds from two amino acids in the protein.

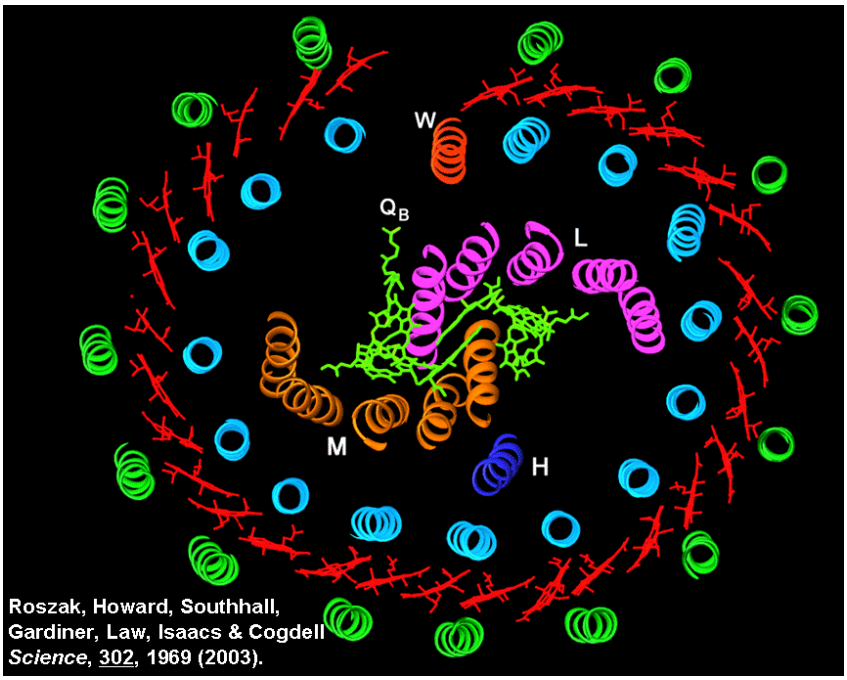

Figure 13 The structure of the LH1/reaction center complex from a purple bacterium.

Figure 15 shows peak shift data at 850 nm for two different samples—solubalized, isolated individual LH2 rings (red circles), and LH2 complexes in contact with each other in an intact membrane (blue squares). The rapid decay of the peak shift is the same in both samples and results from ultrafast energy transfer (or equivalently exciton relaxation) within a single B850 ring. However, only the membrane sample shows a much slower (5 ps) component. It seems very likely that this 5 ps component describes energy transfer between the different LH2 rings in the membrane leading to averaging over the full range of disorder in the sample on this timescale.

Thus the peak shift method, far from being defeated by static energetic disorder, enables its exploitation to reveal microscopic dynamics of complex systems whose linear absorption spectra are often singularly uninformative.

Although the 3PEPS method is quite powerful for studying complex systems, it is not the most powerful technique. For this we turn to two-dimensional optical spectroscopy.

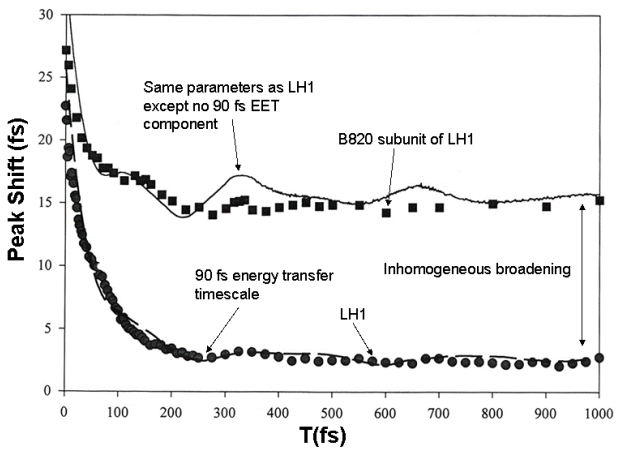

Figure 14 Three-pulse echo peak shift data for the entire LH1 ring [●] and the B820 subunit which contains two BChl molecules [■]. The solid lines are calculated. See text.

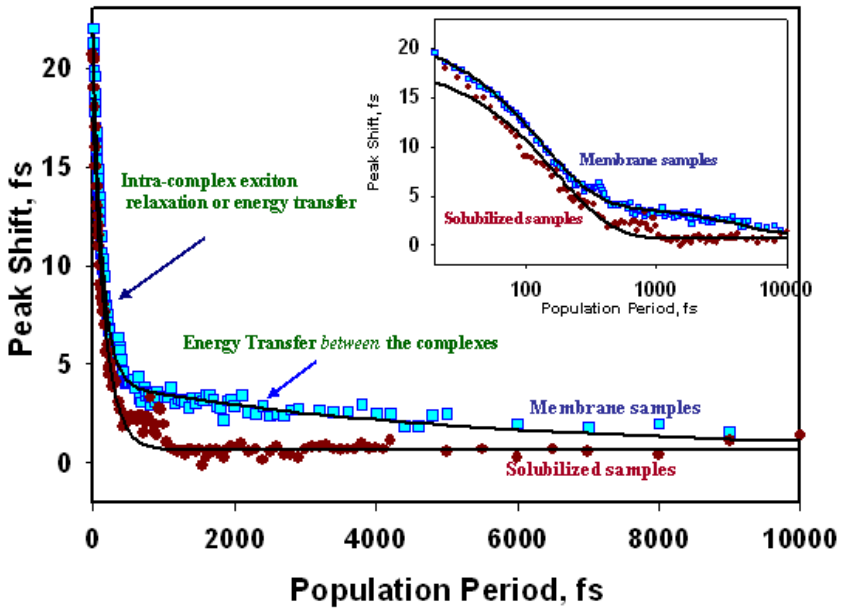

Figure 15 Three-pulse echo peak shift data for isolated LH2 complexes (red) and a membrane sample in which LH2 to LH2 transfer is possible (blue).

4. Two-Dimensional Electronic Spectroscopy

The goal of two-dimensional optical spectroscopy is to characterize the complete signal field as a function of the three time periods involved in a four-wave mixing experiment. Generally, the signal in which the system is in a coherence in the first (τ) and the third (t) time periods and in a population in the middle (T) period is recorded (Figure 8). The 2D spectrum then consists of a plot of $S(\omega_\tau, \mathrm{T}, \omega_t)$ for fixed values of the population time. In other words it shows the correlation between the excitation (ω_τ) and detection (ω_t) frequencies, and how this correlation evolves in time. The sequence of events is depicted in Figure 16, and the experimental arrangement needed to record such a spectrum in Figure 17. In principle the required spectrum could be obtained by scanning both τ and t, and carrying out double Fourier transformation in τ and t of the signal field $S(\tau, \mathrm{T}, t)$. In practice, the signal in the $t-$dimension is obtained by spectral interferometry, i.e. heterodyne detection in the frequency domain with a reference local oscillator (LO). The signal recorded is $\left|E_{sig}(\omega)+E_{LO}(\omega)\exp(-i\omega t_{LO}\right|^2$, and only a single Fourier transform along τ is required to obtain the 2D spectrum.

Figure 18 shows a schematic representation of a 2D spectrum at a fixed value of T. The peaks along the diagonal represent the ordinary linear absorption spectrum. Diagonal elongation of the peaks implies strong correlation between excitation and detection frequencies, in other words, inhomogeneous broadening. If there is no correlation between the excitation and detection frequencies, the peak should be symmetrical—a 2D Lorentzian produces a 'star'-shaped peak, while a 2D Gaussian gives a round peak. Note the 2D spectrum carries sign information—generally ground state bleaching and stimulated emission are represented as positive green to red in Figure 18 and excited state absorption as negative (blue to violet in Figure 18). Peaks off the diagonal are called cross peaks. They have two types of origin: (1) cross peaks arise from electronic coupling between different chromophores. In the case of a electronically coupled dimer, say, with two allowed bands, both molecules contribute to both transitions.

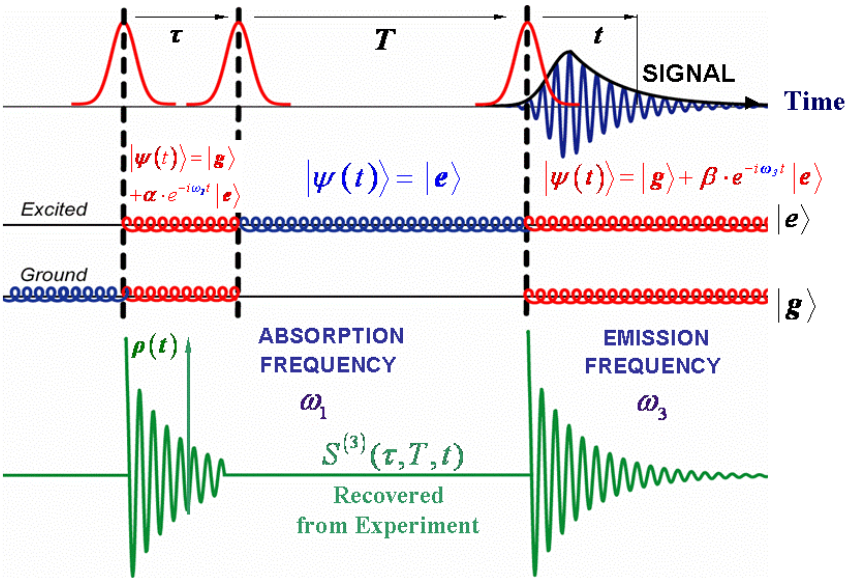

Figure 16 The pulse sequence for two-dimensional electronic spectroscopy. The experiment correlates the frequencies observed during t with those prepared during τ for different (fixed) values of T.

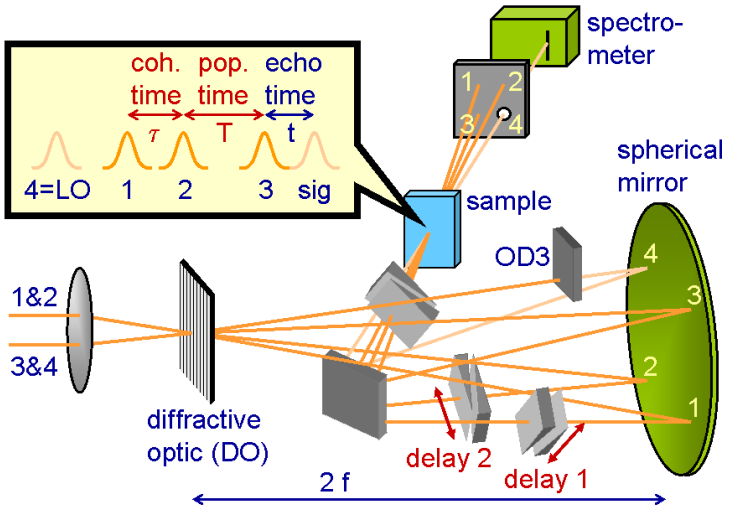

Figure 17 Experimental arrangement for 2D electronic spectroscopy.

This means that absorption into one of the bands will cause bleaching in both of them. Thus excitation in, for example, the higher energy band, will also produce a response in detection at the lower band frequency and a new peak at $\omega_\tau = \omega_{upper}$ and $\omega_t = \omega_{lower}$ will appear. We will demonstrate shortly that such a peak vanishes if there is no coupling between the two monomers. (2) Staying with the dimer example, for larger values of T population initially in the upper state may have relaxed into the lower excited state, again producing a cross peak at $\omega_\tau = \omega_{upper}$ and $\omega_t = \omega_{lower}$.

Figure 19 allows us to make this a little more formal. The dimer system has a single non-degenerate ground state, g, two singly excited states e_1 and e_2, and a doubly excited state, f. Four-wave mixing, as the name implies, involves four light field/matter interactions, and

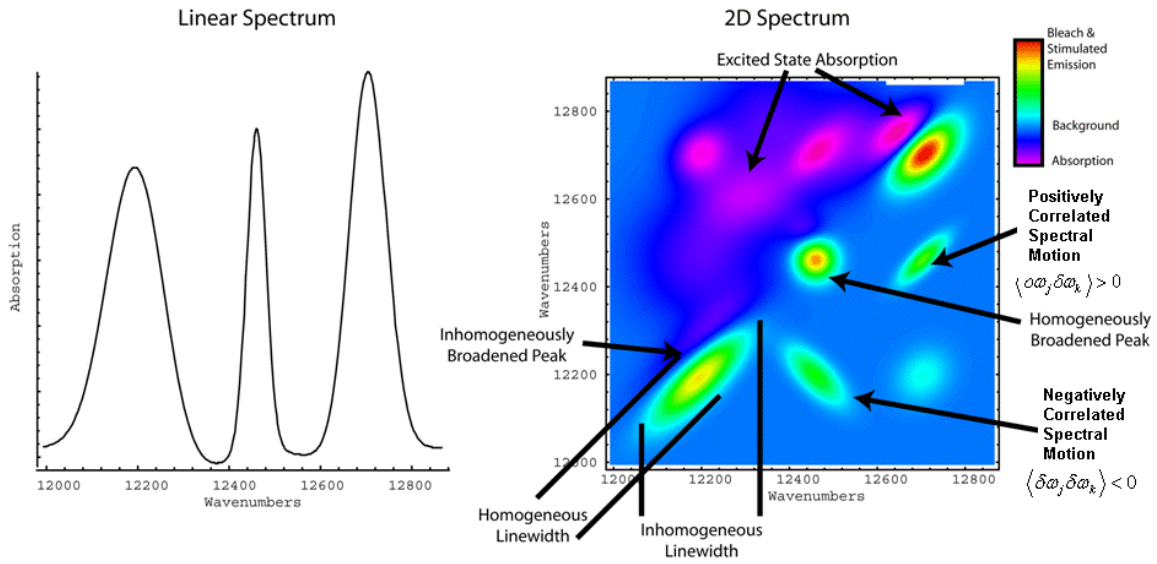

Figure 18 Model spectrum of a three state complex. Left: linear absorption spectrum. Right: 2D electronic spectrum. The linear spectrum gives the diagonal peaks.

the balance between two types of contributions determines the amplitude of the two cross peaks in Figure 19. The first term involves the sequence shown on the left of Figure 19 as either a double-sided Feynman diagram or a ladder diagram. This is an echo sequence with $e_2 g$ during t and ge_1 during τ. (Of course if all four interactions involved only g and e_1, or only g and e_2, only diagonal peaks would be generated). The amplitude of the rephasing sequence depends on μ_{e1} twice and μ_{e2} twice for the S_{12} cross peak, i.e. $<\mu_{e1}^2 \mu_{e2}^2>$ where μ_{e1} is the transition moment for the $g-e_1$ transition and the angle brackets imply orientational averaging for the randomly oriented sample. The existence of the doubly excited (or two-exciton) state f requires that a second sequence be considered as shown on the right of Figure 19. This is excited state absorption and appears with an opposite sign to the first process which involves bleaching/stimulated emission. The Feynman diagram shows the same thing via the unequal number of bra and ket interactions with the fields. The dipole factor, including the sign, associated with this process is $-<\mu_{e1}\mu_{e1f}^2\mu_{e1}>$ with μ_{e1f} the transition dipole for the $e_1 - f$ transition. The amplitude of the S_{12} cross peak is determined by the destructive interference between these two pathways i.e.

$$S_{12} \propto <\mu_{e1}^2 \mu_{e2}^2> - <e_{1}\mu_{e1f}^2 \mu_{e1}> \qquad (6)$$

In the simplest Frenkel Hamiltonian $\omega_{ge1} = \omega_{e2f}$ and $\omega_{ge2} = \omega_{e1f}$. When the coupling goes to zero the right-hand sequence simply amounts to two transitions (g_{e1} twice and g_{e2} twice) on the two molecules because now $\mu_{e1f} = \mu_{e2}$ implying transitions between two independent molecules. Thus the second term in (6) becomes identical to the first and S_{12} vanishes. Cross peaks do not exist for uncoupled chromophores. Knowledge of cross peak amplitude and, in particular, the way in which cross peak amplitude depends on the relative polarizations of the

four optical fields can be used to determine the spatial structure of the system's electronic states, and provide rough atomic structural information.

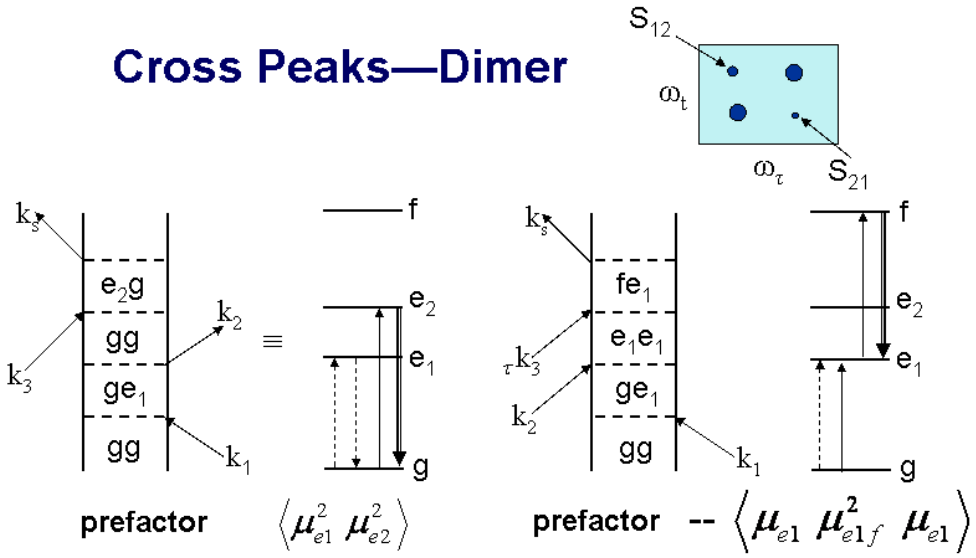

Figure 19 Feynman diagrams and energy level diagrams showing the origin of cross peaks in a dimer at T=0.

Figure 20 shows two experimental 2D electronic spectra for the Fenna-Matthews-Olson complex which contains seven non-equivalent BChl molecules. There are thus seven 1-exciton states and 21 2-exciton states. In the left spectrum of Figure 20, the pulse polarizations have been chosen to discriminate against diagonal peaks to better reveal the cross peaks. For comparison the right spectrum ("all parallel") is dominated by the diagonal peaks.

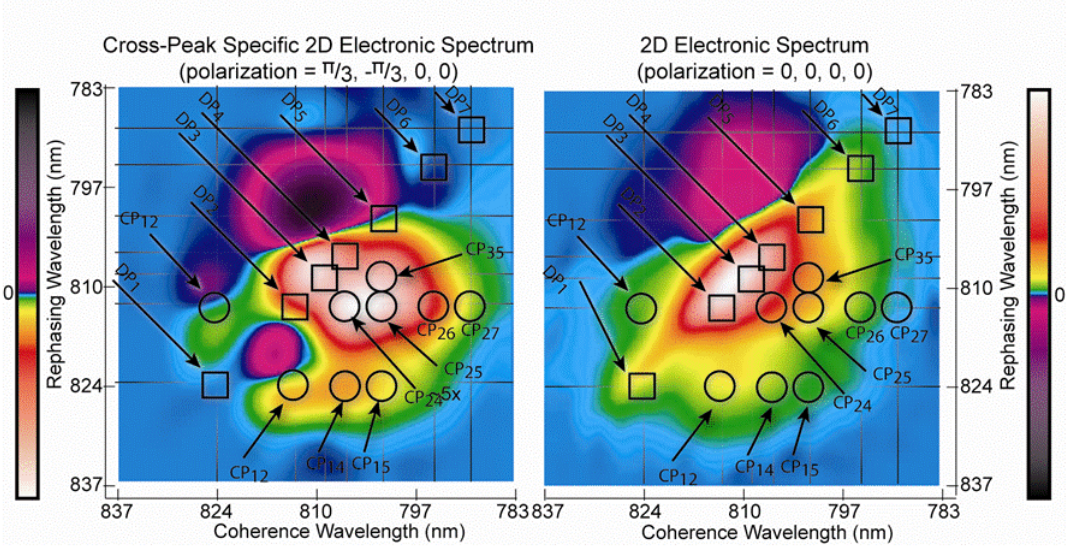

Figure 20 2D spectra of the FMO complex with all parallel polarization (right) and polarization selected to suppress the diagonal peaks (left). The four polarizations are read right to left and describe pulse 1, 2, 3 and signal, respectively.

Figure 20 shows experimental and calculated 2D spectra for the light harvesting complex LH3 (at 77K) which has a structure essentially identical to LH2 discussed earlier, with two rings of 9 and 18 BChl, respectively. In LH3 the spectrum of the strongly

interacting ring of 18 BChl is shifted to peak at 820 nm, while the ring of 9 BChl remains at 800 nm. The clear cross peak developing from 1-5 ps indicates relaxation (energy transfer) from B800 to B820. Strong excited state absorption features also develop on the same timescale, and the B800 diagonal peak eventually disappears. The B800 and B820 diagonal peaks show very different short-time dynamics, with noticeable changes (loss of diagonal character) in the B820 band over the first 50 fs and no discernable change in the B800 band. This is due to the rapid relaxation within the inhomogeneous broadened set of 18 1-exciton states of B820, leading to loss of memory. Transfer within B800 is much slower. Also note the noticeable asymmetry around the diagonal of the B800 diagonal peak. This arises from interference between ground to 1-exciton and 1-exciton to 2-exciton states which have opposite signs. The redistribution of oscillator strength over the ground to 1-exciton and 1-exciton to 2-exciton transitions makes the 2D spectrum extremely sensitive to electronic couplings. If the B800-B800 coupling were zero, the B800 diagonal peak would be symmetrical about the diagonal.

The actual coupling is ~30 cm^{-1} and this produces the clear asymmetry evident in Figure 21. Detailed analysis of the data in Figure 21 confirms earlier conclusions that B800 to B820 energy transfer occurs through dark states which relax to the lower (allowed) levels of B820.

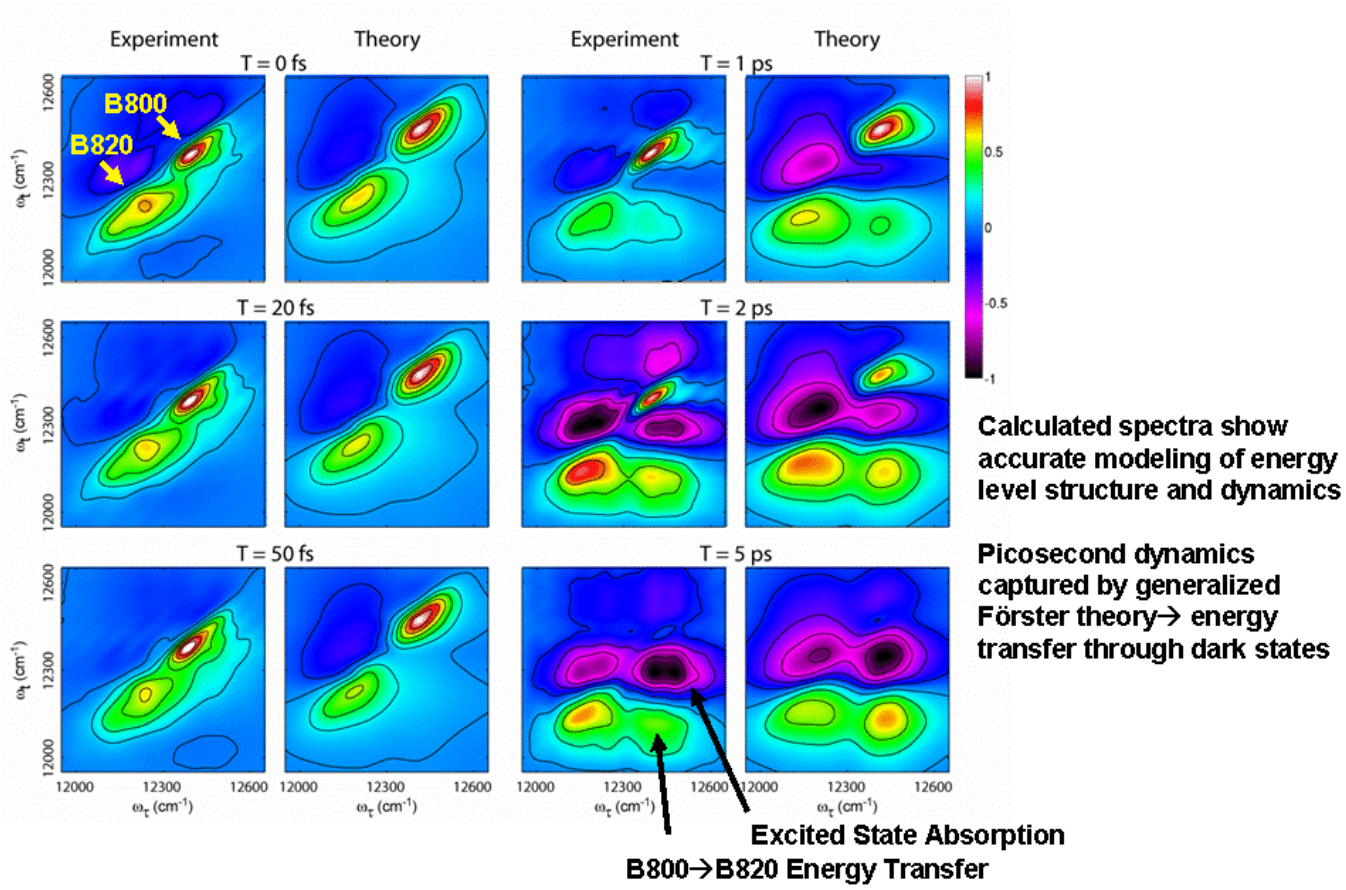

Figure 21 Comparison of measured and calculated 2D spectra for the LH3 complex which is structurally almost identical to LH2 shown in Figure 12.

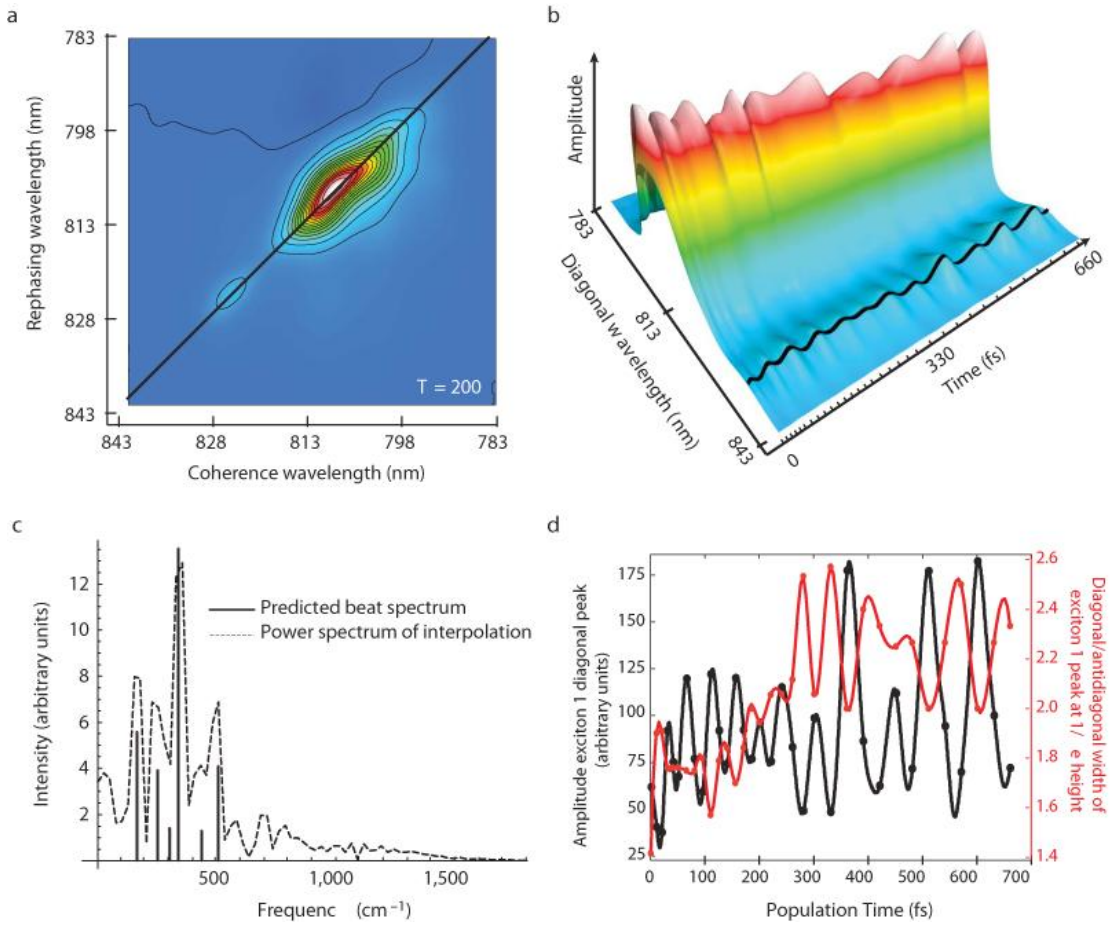

Figure 22 Coherence quantum beating in the FMO complex [62]. (a) The 2D spectrum of the FMO complex measured at T=200 fs and 77 K. (b) Time-evolution of the diagonal sliceof the 2D spectrum. The beating signal of the first exciton peak is emphasized with the solid black line. (c) Comparison between the interpolated power spectrum of this _rst exciton beating signal (dashed curve) and the theoretical beat spectrum predicted by the excitonic energy structure (black stick spectrum). (d) The amplitude of the exciton 1 diagonal peak (black curve) and the ratio of the diagonal to anti-diagonal widths of the peak (red curve). The anticorrelation is a characteristic of excitonic quantum beating [21, 22].

Two-dimensional spectroscopy has been applied to several light harvesting complexes including the most abundant, LHCII. It has revealed energy transfer pathways and mechanisms, spatial landscapes and electronic coupling strengths. These applications have been recently reviewed in reference (7).

A final important aspect of 2D spectroscopy relates to its ability to reveal quantum dynamical aspects of phenomena. This arises fundamentally because 2D spectroscopy is a measurement at the amplitude level whereas most techniques detect the absolute square of the signal field. Consider the evaluation of a quantum superposition

$$\left|\Psi(t)\right\rangle \quad = \quad a\,\exp(-i\omega_1 t)\left|e_1\right\rangle + \; b\,\exp(-i\omega_2 t)\left|e_2\right\rangle$$

The density matrix is thus

$$
\begin{aligned}
|\Psi(t)\rangle\langle\Psi(t)| \;=\; & a|e_1\rangle\langle e_1| + b|e_2\rangle\langle e_2| \\
& + ab^{*}\exp(-i(\omega_1-\omega_2)\,t)\;|e_1\rangle\langle e_2| \\
& + a^{*}b\;\exp(i(\omega_1-\omega_2)\,t)\;|e_2\rangle\langle e_1|
\end{aligned}
$$

The first two terms in equ. (7) reflect populations, while the second two terms describe coherences. 2D spectroscopy can directly measure the phase evolution of coherences and thus directly reveal the presence of quantum coherence as a function of time in a dynamical system. Experiments have shown the presence of remarkably long-lived electronic coherence in photosynthetic light harvesting complexes (Figure 22), and this has become a very active area of research, with connections ranging from protein structure to quantum information and quantum computing.

Acknowledgments

This work was supported by grants from the US National Science Foundation and by the Director, Office of Science, Office of Basic Energy Sciences, of the U.S. Department of Energy under Contract No. DE-AC02-05CH11231 and by the Chemical Sciences, Geosciences and Biosciences Division, Office of Basic Energy Sciences, U.S. Department of Energy under contract DE-AC03-76SF000098. The content owes much to the many remarkable students, post docs, and colleagues involved in my group's work.

References

Useful Texts

1. G.R. Fleming, *Chemical Applications of Ultrafast Spectroscopy* (monograph), Oxford University Press, Oxford, 1986.
2. S. Mukamel, *Principles of Nonlinear Optical Spectroscopy*, Oxford University Press, Oxford, 1995.
3. R. Blankenship, *Molecular Mechanisms of Photosynthesis*, Blackwell Science, Oxford, 2002
4. G. C. Schatz and M. A. Ratner, *Quantum Mechanics in Chemistry*, Prentice Hall, Englewood Clifs, New Jersey, 1993.
5. A. Nitzan, *Chemical Dynamics in Condensed Phases: Relaxation, Transfer and Reactions in Condensed Molecular Systems*, Oxford University Press, Oxford, 2006.
6. B. R. Green and W.W. Parsons (Eds.), *Light-Harvesting Antennas in Photosynthesis*, *Advances in Photosynthesis and Respiration*, v. 13, Kluwer Academic Publishers, Norwell, Massachusetts, 2003.
7. Y-C Cheng and G. R. Fleming, *Dynamics of Light Harvesting in Photosynthesis*, *Annual Review of Physical Chemistry*, (In Press).

Specific References

8. N.F. Scherer, D.M. Jonas and G.R. Fleming, *J. Chem. Phys*. 99 (1993) 153.
9. M. Ben-Nun, R.D. Levine and G.R. Fleming. *J. Chem. Phys.* 105 (1996) 3035.
10. R. Jimenez, G.R. Fleming, P.V. Kumar and M. Maroncelli. *Nature* 369 (1994) 471.
11. T. Joo, Y. Jia, J-Y. Yu, M.J. Lang and G.R. Fleming. *J. Chem. Phys.* 104 (1996) 6089.
12. G.R. Fleming and M. Cho. *Annu. Rev. Phys. Chem.* 47 (1996) 109.
13. M. Cho, J-Y. Yu, T. Joo, Y. Nagasawa, S.A. Passino and G.R. Fleming. *J. Phys. Chem.* 100 (1996) 11944.

14. G.R. Fleming, S.A. Passino and Y. Nagasawa. *Phil. Trans. Roy. Soc. A*, 356 (1998) 389.
15. J-Y. Yu, Y. Nagasawa, R. van Grondelle and G.R. Fleming. *Chem. Phys. Lett.*, 280 (1997) 404.
16. R. Agarwal, A. H. Rizvi, B.S. Prall, J. D.Olsen, C. Neil Hunter, and G. R. Fleming, *J. Phys. Chem. A.*, 106 (2002) 7573.
17. M. Cho, H.M. Vaswani, T. Brixner, J. Stenger and G.R. Fleming, *J. Phys. Chem. B.*, 109 (2005) 10542.
18. T. Brixner, J. Stenger, H. Vaswani, M. Cho, R.E. Blankenship and G.R. Fleming, *Nature*, 434 (2005) 625.
19. D. Zigmantas, E.L. Read, T. Mancal, T. Brixner, A.T. Gardiner, R.J. Cogdell and G.R. Fleming. *PNAS*, 103 (2006) 12672.
20. G. S. Engel, T. Calhoun, E.L. Read, T. K. Ahn, T. Mancal, R. E. Blankenship and G. R Fleming. *Nature* 446 (2007) 782.
21. A.V. Pisliakov, T. Mancal and G.R. Fleming. *J. Chem. Phys*., 124 (2006) 234505.
22. Y-C. Cheng and G. R. Fleming, *J. Phys. Chem. A*, 112 (2008) 4254.